Radio Wave Scattering from Lampposts in Microcell Urban Mobile Propagation Channel

Mir Ghoraishi[1], **Jun-ichi Takada**[2], and **Tetsuro Imai**[3], Non-members

ABSTRACT

The radio wave scattering from lampposts in urban areas is analyzed. The lamppost is modeled as a finite-length conducting cylinder and the approximate theoretical values of its bistatic radar cross section (RCS) are compared to those experimental values obtained from a propagation channel measurement campaign in two urban environments. In the theoretical derivation it is assumed that two waves, direct and ground-reflected, are incident to the lamppost, whereas only direct scattering is assumed due to the directive receiver (Rx) antenna. The CDF of the theoretical RCS of the cylinder and those of the lamppost derived from measurement data exhibit a close agreement.

Keywords: Lamppost, radar cross section, urban propagation channel.

1. INTRODUCTION

Conventional propagation prediction tools, such as ray-tracing algorithms, only account for specular reflections from building wall surfaces and diffractions from building corners and roof-top edges. But this is an oversimplification of the complex architecture of the propagation channel in the urban areas. In fact, not only approximating the interaction of a building wall in the urban areas to a specular reflection is too optimistic for cellular operating frequencies, but also there are many interacting objects other than buildings in the wireless channel in these environments with a collective significant impact to the receiving signal [1]. To improve the accuracy of propagation prediction tools, several researches were accomplished to include the building rough surface scatterings [2],[3],[4]. Moreover, the scattering from trees was addressed in [5],[6]. However, the scattering effect of objects such as lampposts, traffic lights and signboards have not been analyzed or modeled carefully even though their contribution to the channel are considerable [1]. In this paper we analyze the scattering effect of the lamppost in the urban environments by obtaining its radar cross section (RCS) experimentally and analytically. For this purpose we use the experiment results of a measurement campaign in Yokohama, Japan in a microcell scenario [7].

This is done through deriving RCS of the lampposts from measurements in real scenarios in comparison to the analytical results.
Section 2. provides the analytical modeling of the lamppost as a conducting cylinder to get its RCS values. In section 3. coherent and incoherent two-ray incidence models are introduced to take the measured RCS variations into account. In section 4. we introduce the measurement set up and values, whereas section 5. introduces the simulation and its predictions. Section 6. provides discussions and comparisons and finally section 7. is the conclusion.

2. LAMPPOST RCS MODEL

The definition of RCS is as follows [8]: "For a given scattering object, upon which a plane wave is incident, that portion of scattering cross section corresponding to a specified polarization component of the scattered wave." The RCS is usually shown by σ and can be formulated as [9]:

$$\sigma = \lim_{r_r \to \infty} 4\pi r_r^2 \frac{|\mathbf{E}^s|^2}{|\mathbf{E}^i|^2} \tag{1}$$

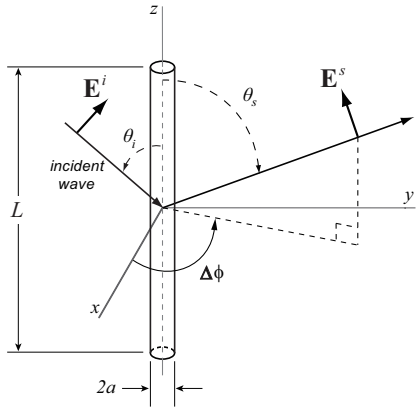

Fig.1: *The incident and scattering parallel electromagnetic wave to a long but finite-length conductor cylinder.*

Manuscript received on January 3, 2008 ; revised on June 13, 2008.

[1]The author is with The Center for Research and Development of Educational Technology Tokyo Institute of Technology 2-12-1-W9-108 Ookayama, Meguro-ku, Tokyo 152-8552, Japan , E-mail:

[2]The author is with International Development Engineering Department Tokyo Institute of Technology 2-12-1-W9-108 Ookayama, Meguro-ku, Tokyo 152-8552, Japan, E-mail:

[3]The author is with R&D Center, NTT DOCOMO, INC., 3-5 Hikarino-oka, Yokosuka-shi, Kanagawa 239-8536, Japan, E-mail:

where $|\mathbf{E}^s|^2$ is the power per unit area in scattered wave at the receiver (Rx) antenna which is in the polarization of the Rx antenna, $|\mathbf{E}^i|^2$ is the power per unit area in the wave incident on the scatterer and r_r is the scatterer to Rx separation.
To get the analytical RCS of the lamppost we approximate it to a long but finite-length conductor cylinder. The approximated theoretical value of the RCS for a perfect conductor finite-length cylinder of circular cross section can be derived by calculating the induced current on the surface of the cylinder. It is formulated as a function of the incident and scattering angles [10]:

$$\sigma = \frac{4L^2 \sin^2\theta_s}{\pi \sin^2\theta_i} \left\{ \frac{\sin[\frac{kL}{2}(\cos\theta_s + \cos\theta_i)]}{\frac{kL}{2}(\cos\theta_s + \cos\theta_i)} \right\}^2 \cdot \left| \sum_{n=-\infty}^{\infty} (-1)^n e^{jn\Delta\phi} \frac{J_n(ka\sin\theta_s)}{H_n^{(2)}(ka\sin\theta_i)} \right| \quad (2)$$

where L and a are the cylinder length and radius respectively with its axis of symmetry along the z axis. Moreover θ_i and θ_s are the incident and scattering waves co-elevations and $\Delta\phi$ is the azimuth difference between the incident and scattering waves. J_n and $H_n^{(2)}$ represent Bessel function of the first kind and Hankel function of the second kind respectively.
Figures 2 and 3 show the cylinder RCS variations as a function of coelevation θ_i and azimuth difference $\Delta\phi$ respectively, for which $L = 6.5\ m$, $a = 0.08\ m$, and $\theta_s = 90°$. It is observed that the cylinder RCS diminishes rapidly as the incident coelevation changes from 90° (horizontal incidence), whereas RCS variations due to the azimuth difference is small except for the backscattering zone. Consequently, in the next section we will address the lamppost RCS variations in the urban areas by introducing a two ray model which imposes the coelevation variations in the superimposed incident wave.

3. TWO-RAY INCIDENCE MODEL

For the incident wave to the lamppost we use the two-ray model [11], [12]. That is we consider the direct incident wave from the transmitter (Tx) antenna with the coelevation of $\theta_{id} = 90°$ and the ground-reflected incident wave with a coelevation of θ_{ig} as is illustrated in Fig. 4. Here we only consider the direct scattering wave, more discussions on this will be provided in section 5.

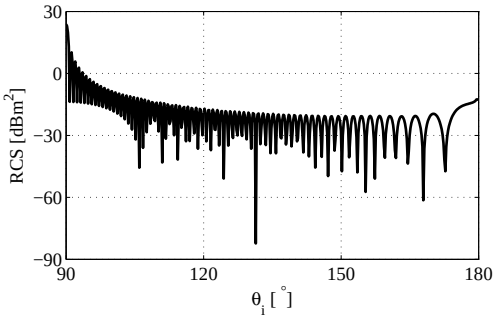

Fig.2: *The RCS of a conductor cylinder as a function of incident wave coelevation θ_i, for $L = 6.5\ m$, $a = 0.08\ m$, $\theta_s = 90°$ and $\Delta\phi = 0$.*

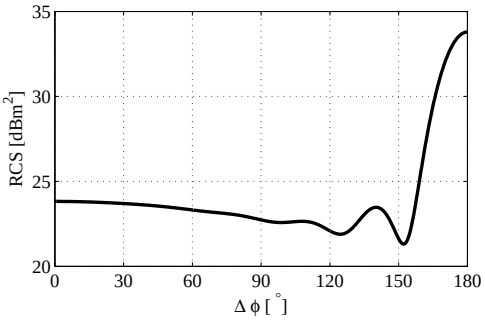

Fig.3: *The RCS of a conductor cylinder as a function of incident and scattering waves azimuth difference $\Delta\phi$, for $L = 6.5\ m$, $a = 0.08\ m$, $\theta_i = 90°$ and $\theta_s = 90°$.*

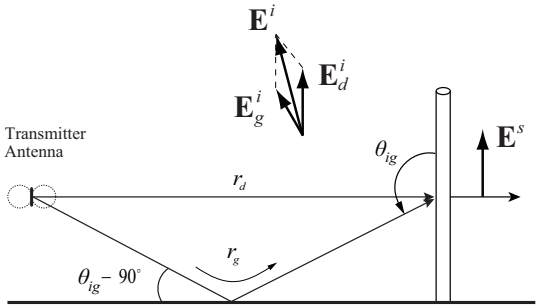

Fig.4: *Two incident paths transmitted by a dipole half wavelength antenna at the cylinder.*

3.1 Coherent waves

When the two incident waves coherently impinge at the lamppost, the composed incident angle is given by the superposition of two propagation vectors of the direct incident wave and the ground-reflected wave. As the Tx antenna is a half wavelength vertically installed dipole, the transmitted signal is vertically polarized (θ component in the spherical coordinates) and there is not any radiation along horizontal polarization vector (ϕ component). However, due to the grazing angle of the ground-reflected wave, the electromagnetic field at the reflection point includes a parallel (to the ground) component. Having the Fresnel parallel $R_\parallel$ and vertical $R_\perp$ coefficients for the ground, the ground-reflected electromagnetic field at the incident point can be calculated as:

$$E^i_{g\parallel} = E_0\, h_\theta(\theta_{ig})\, R_\parallel \frac{e^{-jkr_g}}{r_g} \sin(\theta_{ig} - 90) \quad (3)$$

$$E^i_{g\perp} = E_0\, h_\theta(\theta_{ig})\, R_\perp \frac{e^{-jkr_g}}{r_g} \cos(\theta_{ig} - 90) \quad (4)$$

in which E_0 is the equivalent electric field radiated by the isotropic antenna, r_g is the traveling distance for the ground-reflected wave and h_θ is the dipole field pattern defined as:

$$h_\theta(\theta) = \frac{\cos[\frac{\pi}{2}\cos(\theta)]}{\sin(\theta)} \tag{5}$$

moreover the ground Fresnel coefficient for parallel and vertical polarizations $R_\parallel$ and $R_\perp$ depend on relative dielectric constant of the ground ϵ_r and the grazing angle according to

$$R_K = \frac{\cos(\theta_{ig}-90) - k\sqrt{\epsilon_r - \sin^2(\theta_{ig}-90)}}{\cos(\theta_{ig}-90) + k\sqrt{\epsilon_r - \sin^2(\theta_{ig}-90)}} \tag{6}$$

where $k = 1/\epsilon_r$ for $R_K = R_\perp$ and $k = 1$ for $R_K = R_\parallel$. The relative dielectric constant is $\epsilon_r = \epsilon'_r - j60\lambda\sigma$, in which the values for relative permittivity ϵ'_r and conductivity σ for an average ground are 15 and 5×10^{-3} $\mho$/m respectively [13], and λ is the operating wave-length. For grazing angles however the reflection coefficients can be approximated to $R_\parallel = R_\perp = -1$ [11],[12].

On the other hand, for the direct incident wave, the propagation direction is horizontal and the following relations exist:

$$E^i_{d\parallel} = E^i_{d\,\phi} = 0 \tag{7}$$

$$E^i_{d\perp} = E^i_{d\,\theta} = E_0\,\frac{e^{-jkr_d}}{r_d} \tag{8}$$

where r_d is the the traveling distance for the direct incident wave. The incident angle of the total electric field can be obtained from superposition of the two incident waves that is:

$$\theta_i = \frac{\pi}{2} + \tan^{-1}\left\{\frac{E^i_{d\parallel} + E^i_{g\parallel}}{E^i_{d\perp} + E^i_{g\perp}}\right\} \tag{9}$$

Fig. 5 shows the coelevation of the superposed incident wave as a function of the ground-reflected wave coelevation. Also in Fig. 6 the RCS of the cylinder obtained from the superposed incident wave is illustrated. It is observed that the RCS increases for grazing ground reflections. The reason can be understood by inspecting Fig. 5, in which for grazing ground reflection coelevations the coelevation of the superposed incident wave decreases back toward 90°. In Fig. 6 the total coherent RCS using $R_\parallel = R_\perp = -1$ is also added for comparison. It is observed that the total RCS range using average ground reflection coefficients and $R_\parallel = R_\perp = -1$ does not show any significant difference. As a consequence and for the sake of simplicity, we will use these coefficients in the simulations discussed later in this work.

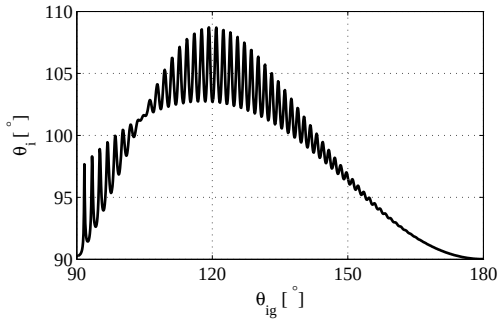

Fig.5: *Incident coelevation angle of the superposed direct and ground-reflected waves as a function of ground reflection coelevation.*

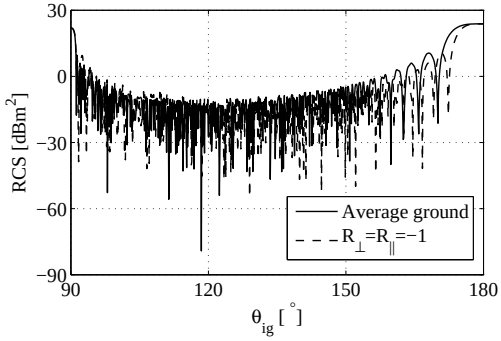

Fig.6: *The total RCS of the conductor cylinder in which the coherent direct and ground-reflected waves are impinged as a function of ground reflection coelevation.* $L = 6.5$ *m,* $a = 0.08$ *m,* $\theta_s = 90°$.

3.2 Incoherent waves

It is observable that the total incident and scattering waves can be obtained as:

$$\mathbf{E}^i = \mathbf{E}^i_d + \mathbf{E}^i_g \tag{10}$$

$$\mathbf{E}^s = \mathbf{E}^s_d + \mathbf{E}^s_g \tag{11}$$

Where $\mathbf{E}^s_d$ and $\mathbf{E}^s_g$ are the scattering electric fields due to direct and ground-reflected incident waves respectively. According to the definition, the total RCS σ_t is:

$$\sigma_t = \lim_{r_r\to\infty} 4\pi r_r^2\,\frac{|\mathbf{E}^s_d + \mathbf{E}^s_g|^2}{|\mathbf{E}^i_d + \mathbf{E}^i_g|^2} \tag{12}$$

In the incoherent incident and scattering, the total incident power is the incoherent superposition of the two incident waves and scattered waves are also incoherently added. The total RCS for this case therefore is equal to:

$$\sigma_t = \lim_{r_r\to\infty} 4\pi r_r^2\,\frac{|\mathbf{E}^s_d|^2 + |\mathbf{E}^s_g|^2}{|\mathbf{E}^i_d|^2 + |\mathbf{E}^i_g|^2} \tag{13}$$

After simple manipulations, the total RCS expression turns to the following formula:

$$\sigma_t = \frac{\sigma_d + \Gamma_g \cdot \sigma_g}{1 + \Gamma_g} \tag{14}$$

Table 1: *Experiments Specifications*

f_c		3.35 GHz
Tx	Signal	BPSK with PN-9 sequence
	Chip rate	50 Mcps
	Power	40 dBm
	Antenna	Sleeve (2.2 dBi)
	Antenna height	3 m
Rx	Antenna	Patch array (24.5 dBi), 10° beamwidths in azimuth and elevation sidelobe level -26 dB
	Antenna height	3 m
	Azimuth scan	3° step (120 points for full azimuth)
Tx-Rx configuration		60 m separated, line-of-sight (LoS)

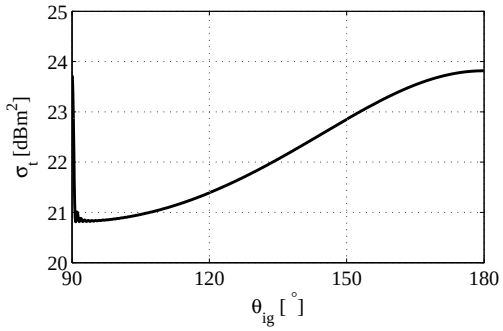

Fig.7: *The total RCS of the conductor cylinder for the incoherent direct and ground-reflected waves as a function of ground reflection coelevation.* $L = 6.5$ *m,* $a = 0.08$ *m,* $\theta_s = 90°$.

where the RCS for the direct incident wave separately is σ_d and that of the ground reflection is σ_g. Moreover, Γ_g is the ratio between the incident ground reflection power and the incident direct path power: $\Gamma_g = |\mathbf{E}_g^i|^2/|\mathbf{E}_d^i|^2$. This factor is different from Fresnel coefficient as the direct wave and the ground-reflected wave travel different distances to the scatterer.
Fig. 7 illustrates the total incoherent RCS for a cylinder of $L = 6.5$ m, $a = 0.08$ m, $\theta_s = 90°$ and $\Delta\phi = 0$. It is observable that for the incoherent case, by increasing the incident ground-reflected coelevation the total RCS of the cylinder changes no more than a few dBs.

4. MEASUREMENTS

In this section the measurement campaign in urban areas is described. We will derive the RCS of a number of lampposts in two locations of urban areas in Yokohama, and then will compare the values with those obtained from two ray models of section 3.

4.1 Set up and scenario

Table 1 shows the specifications of the experiments. The detailed description of the measurements, data analysis and scatterer identifications can be found in [1],[7]. Measurements were accomplished in a street of 26 m wide (location 1) and another nearby street of 18 m wide (location 2) in the dense urban areas of Yokohama, Japan. The directional data was acquired and by investigating the azimuth-delay-power spectrum we were able to identify the scatterer objects in azimuth-delay domain. The significance of the scattering from identified objects such as lamppost, signboard, etc. is estimated to be up to 40% of the non-line-of-sight received power [1].
The important relevant point is that the Tx dipole antenna was rotated with a diameter of 0.5 m and constant rotation speed of 5 rpm to create dynamic uncorrelated fading [1],[7]. As a consequence, the transmitted multipath are averaged. We use this to choose the appropriate two-ray model in the simulations. In the next subsection we will use the outcome of the lamppost identification to get its RCS in each of the measurement locations.

Table 2: *The RCS of lampposts of the location 1, measurement points 1 and 2 (P1, P2).*

	σ_m $[m^2]$	
No	P1	P2
1	114	91
2	NA	114
3	199	122
4	81	116
5	117	150
6	131	196

Table 3: *The RCS of lampposts of the location 2, measurement points 1, 2 and 3 (P1, P2, P3).*

	σ_m $[m^2]$		
No	P1	P2	P3
1	47	65	82
2	80	89	102
3	67	69	72
4	88	46v	12
6	14	24	81
7	53	15	43
8	50	NA	47
9	61	95	69
10	40	30	29
11	48	67	68
12	22	31	NA
13	99	46	45

4.2 Measured RCS

For location 1, the number of identified lampposts is 6, whereas 13 lampposts were identified in location 2. To obtain the RCS of lampposts from the mea-

surement data we can use the radar equation [14]:

$$P_{ra} = \frac{P_{ta} G_t G_r \lambda^2}{(4\pi)^3 r_t^2 r_r^2} \ \sigma_m \qquad (15)$$

where:

P_{ta} : transmitted power at the Tx antenna,
P_{ra} : received power at the Rx antenna,
G_t : gain of the Tx antenna,
G_r : gain of the Rx antenna,
r_t : distance between Tx antenna and the scatterer,
r_r : distance between Rx antenna and the scatterer,
λ : operating wave-length,
σ_m : RCS of the scatterer obtained from measurement data.

Table 2 shows the the RCS of the identified lampposts in location 1 derived for 2 measurement points, and Table 3 shows the RCS of the identified lampposts in location 2 obtained for 3 measurement points. Remarkable is that the lampposts in each measurement location are uniform whereas the shape of lampposts in location 1 is different from those of location 2. Therefore, as the RCS value is a function of the scatterer's shape, the variations of RCS in each table is unexpected.

4.3 Analytical RCS values

Neglecting multipath effect and considering the equal Tx antenna and Rx antenna heights, it can be assumed that the incident and scattered waves are both horizontal. In this case the RCS, σ, can be calculated using $\theta_i = \theta_s = 90°$, $\Delta\phi = 0$, $a = 0.08$ m, $L = 6.5$ m for location 1 and $a = 0.07$ m and $L = 4.5$ m for location 2. With these parameters the value of σ for lampposts of location 1 is 241 m^2 and of location 2 is 101 m^2. These values however can not explain the variations in measured RCS of tables 2 and 3. In the next section, we employ those models of section 2. to reproduce these variations.

5. SIMULATION

Variations of the measured RCS from the analytical values of section 4.3 can be due to changes in the coelevation of the incidence, and the incident and scattering azimuth differences. The former can be modeled according to analyses in section 3. whereas the latter can be assumed a random value. In the simulations the two-ray model is considered for the incidence and only direct scattering wave is accounted because the Rx antenna is directive and the ground reflection is not within the Rx antenna beam-width as the scenario is illustrated in Fig. 8. Moreover even though incident multipath superpose coherently at the scatterer, as a consequence of averaging the multipath by rotating the Tx antenna in the experiments, the superposition of the incident multipath at the scatterer in incoherent. The RCS values of the incoherent two-ray model σ_t for the lampposts of location 1 and of location 2 are presented in figures 9 and 10 respectively as a function of ground-reflected wave coelevation in linear scales. It is observed that consistent with what inferred from the measurement scenario, the range of these values are close to those of tables 2 and 3. This is in contrast to two-ray coherent model discussed in section 3.1 which predicts values much smaller than measured lamppost RCS. To investigate the goodness of the exercised model we conducted a Monte-Carlo simulation by assuming that lampposts are distributed randomly in each of the measurement locations. Hence it is assumed that $\Delta\phi$ is uniformly distributed over the interval $[0, 150°]$, because the measurement is in line-of-sight scenario and no lamppost can locate in between Tx and Rx to make a larger $\Delta\phi$. The ground reflection coelevation is assumed in the interval $[90°, 180°]$, however its most probable region is assumed $[93°, 150°]$ corresponding to a Tx to the lamppost separation of 120 m to 3 m. Moreover, simulation results show that for location 1 best results are obtained with %90 of the lampposts in this region, whereas this value for location 2 is %80.

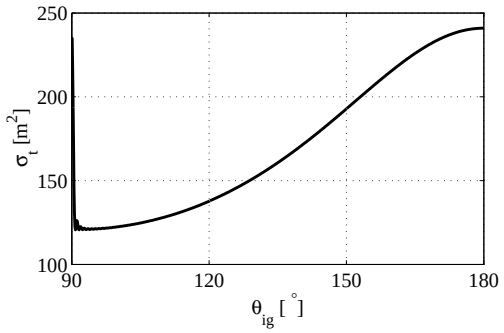

Fig.9: *The total RCS value σ_t for lampposts of location 1 as a function of the incident angle of ground reflection wave θ_{ig}.*

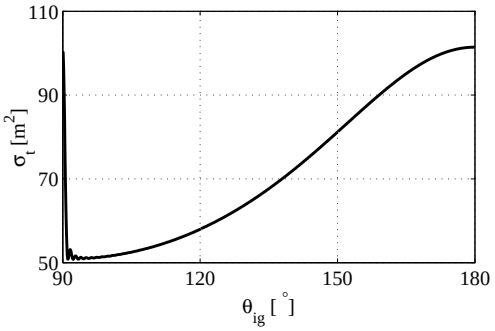

Fig.10: *The total RCS value σ_t for lampposts of location 2 as a function of the incident angle of ground reflection wave θ_{ig}.*

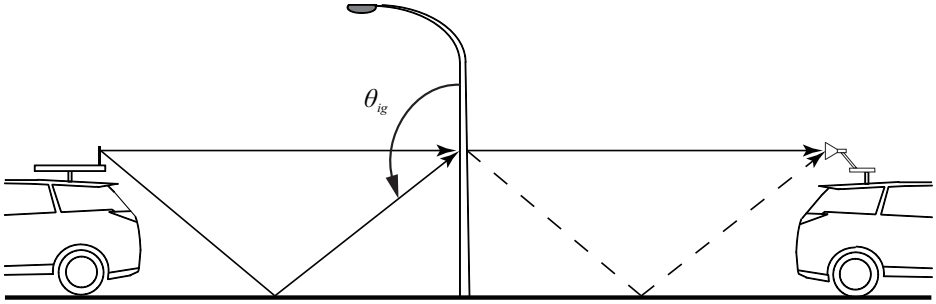

Fig.8: *Two incident waves at the lamppost, whereas only direct scattering wave is considered as the Rx antenna is directive.*

6. DISCUSSION

As it was expressed in previous section, the incoherent two-ray model was employed amid coherent scattering in the channel because the Tx antenna was rotated during the measurements to average the transmitted multipath. This will cease to incoherent superposition of the incident multipath at the scatterers. In addition, the RCS values obtained from the incoherent two-ray incidence model present a close match to the measured values in the urban environments. The CDF of the analytical RCS values σ_t derived from Monte-Carlo simulations and those of measured values σ_m are presented in figures 11 and 12 for locations 1 and 2 respectively. It is observed that by using the incoherent two-ray model for the incident wave to the lamppost, an excellent agreement between the CDFs of the measured and simulated values are achievable.

Small differences in the low RCS values for location 2 in Fig. 12 is observable which may be explained by a *two-ray scattering* model. Earlier we argued that we do not consider the two-ray model for the scattering, nonetheless there can be some lampposts with the scattering ground reflections within the beam-width of the Rx directive antenna. If two waves (the direct and the ground-reflected) were superimposed destructively at the Rx [12], a lower measured scattering power at the Rx would be observed and consequently the measured RCS would be smaller.

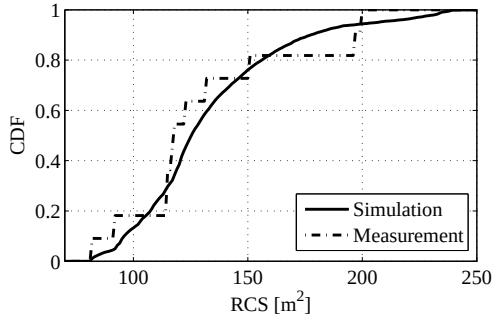

Fig.11: *The CDF of the total RCS for the lampposts of location 1.*

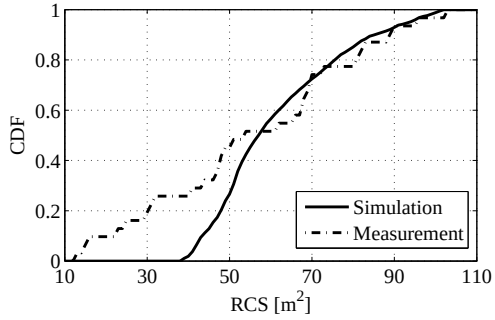

Fig.12: *The CDF of the total RCS for the lampposts of location 2.*

7. CONCLUSION

The study of scattering from objects such as lampposts is a critical issue in the analysis of the wireless propagation channel in the urban environments. Lampposts are widely used in such areas and exhibit a significant potential for scattering radio waves.

In this paper, we employed a two-ray incidence model to explain the radio wave scattering properties of the lampposts in the urban wireless radio channel. A comparison of the CDF of the RCS obtained from simulation and those calculated from the measurement data shows that the two-ray incidence model can predict the scattering of radio waves from lampposts in the urban areas.

References

[1] M. Ghoraishi, J. Takada, T. Imai, "Identification of scattering objects in microcell urban mobile propagation channel," *IEEE Trans. on Antennas and Propagation,* Vol. 54, No. 11, pp 3473-3480, Nov. 2006.

[2] H. Budiarto, K. Horihata, K. Haneda, J. Takada, "Experimental study of non-specular wave scattering from building surface roughness for the mobile propagation modeling," *IEICE Trans. on Communications*, Vol. E87-B, No.4, pp. 958-966, April 2004.

[3] P. Pongsilamanee, H. Bertoni, "Specular and nonspecular scattering from building facades," *IEEE Trans. on Antennas and Propagation*, Vol. 52, No. 7, pp. 1879-1889, July 2004.

[4] V. Degli-Esposti, F. Fuschini, E. Vitucci, G. Falciasecca, "Measurement and modelling of scattering from buildings," *IEEE Trans. on Antennas and Propagation*, Vol. 55, No. 1, pp. 143-153, Jan. 2007.

[5] N. Blaunstein, D. Censor, D. Katz, "Radio propagation in rural residential areas with vegetation," *Progress In Electromagnetics Research*, PIERS 40, 131.153, 2003.

[6] Y. de Jong, M. Herben, "A tree-scattering model for improved propagation prediction in urban microcells," *IEEE Trans. on Vehicular Technology*, Vol. 53, No. 2, pp. 503-513, March 2004.

[7] M. Ghoraishi, J. Takada, T. Imai, "Microcell urban propagation channel analysis using measurement data," *Proc. of IEEE Vehicular Technology Conf. (VTC'05 Fall)*, Vol. 3, pp. 1728-1731, Sept. 2005.

[8] "IEEE standard definitions of terms for antennas Antennas and Propagation," IEEE Standards 145-1983, June, 22, 1983.

[9] A. Bhattacharyya, D. Sengupta, *Radar Cross Section Analysis and Control*, Artech House, 1991.

[10] V. DiCaudo, W. Martin, "Approximate solution to bistatic radar cross section of finite length, infinitely conducting cylinder," *IEEE Trans. on Antennas and Propagation*, AP-14, No. 5, pp. 668-669, Sept. 1966.

[11] H. Xia, H.L. Bertoni, L.R. Maciel, A. Lindsay-Stewart, R. Rowe, "Radio propagation characteristics for line-of-sight microcellular and personal communications," *IEEE Trans. on Antennas and Propagation,* Vol. 41, No. 10, pp. 1439-1447, Oct. 1993.

[12] R. Vaughan, J. Bach Andersen, *Channels, Propagation and Antennas for Mobile Communications*, The IEE Press, 2003.

[13] W. Jakes (Editor), *Microwave Mobile Communications,* Wiley-IEEE Press, 1994.

[14] E. Knott, J. Shaeffer, M. Tuley, *Radar Cross Section,* Artech House, 1985.

Mir Ghoraishi received B.E. from Isfahan University of Technology, Esfahan, Iran, and M.E. from Amirkabir University of Technology, Tehran, Iran, both in electrical engineering in 1993 and 1999 respectively. In 1999 he entered Tokyo Institute of Technology for Ph.D. course where he is a swenior researcher from 2004.

His research interests are radio channel analysis and signal processing fro wireless communication systems and wireless positioning and tracking. He is a member of the Institute of Electrical and Electronics Engineering (IEEE) and the Institute of Electronics, Information and Communication Engineers of Japan (IEICE).

Jun-ichi Takada received the B.E., M.E., and D.E. degrees from the Tokyo Institute of Technology, Tokyo, Japan, in 1987, 1989, and 1992, respectively. From 1992 to 1994, he was a Research Associate Professor with Chiba University, Chiba, Japan. From 1994 to 2006, he was an Associate Professor with Tokyo Institute of Technology. Since 2006, he has been a Professor with Tokyo Institute of Technology.

His current interests are wireless propagation and channel modeling, array signal processing, UWB radio, cognitive radio, applied radio instrumentation and measurements, and ICT for international development. Dr. Takada is a member of IEEE, IEICE, ACES, and the ECTI Association Thailand.

Tetsuro Imai was born in Tochigi, Japan, in 1967. He received his B.S. and Ph.D. degrees from Tohoku University, Japan, in 1991 and 2002, respectively. He joined the Wireless System Laboratories of Nippon Telegraph and Telephone Corporation (NTT), Kanagawa, Japan, in 1991. Since then, he has been engaged in the research and development of radio propagation and system design for mobile communications.

He is now Manager of the Radio Access Network Development Department, NTT DOCOMO, INC., Kanagawa, Japan. Dr. Imai is a member of the Institute of Electrical and Electronics Engineering (IEEE) and the Institute of Electronics, Information and Communication Engineers of Japan (IEICE).